HEFAT2012
9th International Conference on Heat Transfer, Fluid Mechanics and Thermodynamics
16 – 18 July 2012
Malta

WAKE SIMULATIONS IN SHALLOW FLOWS

Nasif G.*, Barron R. and Balachandar R.
*Author for correspondence
Department of Mechanical, Automotive and Materials Engineering,
University of Windsor,
Ontario, Canada,
E-mail: nasifg@uwindsor.ca

ABSTRACT

Three-dimensional numerical modeling using Detached Eddy Simulation (DES) has been carried out to study the characteristics of shallow wake flow. The features of shallow wake flows are highly dependent on the bed characteristics, the free surface and the non-uniform approaching flow velocity profile. An approaching flow with fully developed boundary layer was employed to model the effect of the shallow flow. The shallow wake is generated by introducing a disturbance in the form of a bluff body placed in an open channel. A sharp-edged bluff body is used to reduce the flow sensitivity to Reynolds number and maintain a constant position for boundary layer separation. The flow field structure in the wake i.e., the mean and turbulence characteristics, are examined and compared at different downstream locations to evaluate the effect of vertical variability from the bed. Available experimental data have been used to validate the computational results.

INTRODUCTION

Turbulent shallow water flows are often encountered in nature e.g., wide rivers, lakes, estuaries, shallow coastal waters, stratified flow and atmospheric flow. A proper understanding of shallow wake flow and its transport capacity would be beneficial in a number of cases, e.g., the tendency for pollutants to be trapped in the lee of islands or headlands, nutrient accumulation, or biological activity of various aquatic specious. It would also aid in weather modelling as the waterbeds and marshlands play a crucial role in controlling the local weather [1]. In a shallow or bounded flow, the length scales in both the horizontal and transverse directions are much greater than in the vertical direction [2]. The flow is a boundary layer type, the bed imparts vertical shear while the free surface acts as a stress-free weak boundary. The shallow wakes occur when such flow is destabilized by a sudden change of topology, such as by introducing a horizontal shear (bluff body) or deceleration of the flow. The vertical shear helps to dissipate the kinetic energy and stabilizes the wake flow. By contrast, in the deep wake, the flow is always inviscidly unstable due to the absence of the vertical shear.

The bed friction effect is one of the important factors that identify the features of shallow wake flow. This effect is modelled as a stability parameter $S = f(C_f, D, H)$ which accounts for the influence of stabilization arising from bed friction and the destabilization in the near wake due to the horizontal shear flow. The bed effect might either suppress the vortex shedding or cause it to become intermittent if the stability number exceeds a critical value. The friction effect reduces the entrainment of the surrounding fluid into the wake, arrests the growth of the wake, and subsequently weakens the interaction between the shear layers and stabilizes the wake at near bed locations [3]. The recirculation flow behind the bluff body is completely suppressed at near bed locations. Streamwise directed positive velocities have also been experimentally observed in the wake centreline near the bed [4].

NOMENCLATURE

C_f	[-]	Bed skin friction coefficient
D	[m]	Width of the bluff body
H	[m]	Depth of flow
k	[m^2/s^2]	Turbulent kinetic energy
DES	[-]	Detached Eddy Simulation
RANS	[-]	Reynolds Averaged Navier-Stokes
S	[-]	Stability parameter
St	[-]	Strouhal number
$\mathbf{U}_\infty$	[m/s]	Free surface velocity magnitude
U	[m/s]	Velocity magnitude
U, V, W	[m/s]	Velocity components
u, v, w	[m/s]	Velocity fluctuation components
$\boldsymbol{w}$	[1/s]	Vorticity magnitude
X	[m]	Cartesian axis direction
Y	[m]	Cartesian axis direction
Z	[m]	Cartesian axis direction
$Z_{0.5}$	[m]	Wake half width

Special characters

δ	[-]	Boundary layer thickness
ω	[1/s]	Specific turbulent dissipation rate (or turbulent frequency)

Subscripts

c, deficit	Centreline deficit
deficit	Deficit
rms	Root mean square
s	Upstream
x, y, z	Component directions

Three categories of shallow wake flow pattern have been identified in [5]; vortex street, steady and unsteady wake bubble flows, and the stability number is central to defining the limits between these modes. If the perturbation is due to the alternate separation of the shear layer ($S \leq 0.2$), the shallow wake resembles the von Karman vortex street. If the bed friction effect increases, the shear layers separate simultaneously, a steady bubble region is formed immediately downstream of the body, and the degree of stability of this region will identify the steadiness or unsteadiness of the bubble wake flow.

The formation of a large-scale vortex street involves upward ejection of fluid through its centre, which eventually lead to a horizontal vortex that induces significant distortion of the free surface [6]. The strength of this vortex is an order of magnitude smaller than the large vortex street. The existence of the upward axial flow along the core of the vortex is also observed by using a dye visualization technique [7]. A technique of high-image-density particle image velocimetry was used in [8] to investigate the space-time development of the instantaneous flow patterns for shallow-water wake. The study provided evidence for the presence of the quasi-two-dimensional and three-dimensional vortical structures. The vorticity of the three-dimensional pattern can exceed that of the quasi-two-dimensional pattern by a factor of two.

The interaction between the non-uniform approaching velocity and the front of the bluff body creates a variation in stagnation pressure along the body. Consequently, a horseshoe vortex tube is generated near the channel bed and stretched downstream along the sides of the body. A visualization study of the wake structure behind a circular cylinder was conducted in [9]. They found a vertical oscillation of the shear layer at the sides of the body, which was attributed to the presence of a horseshoe vortex wrapping around the body.

Large eddy simulations (LES) have been used to evaluate the flow features of the near wake behind a cylinder for a wide range of Reynolds numbers [10]. LES provides good agreement with experimental data in describing the Reynolds stresses and the mean flow. However, in the close proximity of the cylinder at low Reynolds numbers, all simulations converge to mean velocity profiles that are different from the experimental results. A combined PIV measurements and Direct Numerical Simulation (DNS) study was conducted to investigate the effect of Reynolds number on the flow characteristics of the cylinder wake at transitional Re = 3900 and at a higher Re = 10,000 [10]. The flow statistics changed significantly with the change of Reynolds number, the principle features of all turbulence quantities moved upstream with increasing Reynolds number. The shear layer instability was found to be significantly influenced by Reynolds number.

The objective of the present study is to obtain further information on the shallow wake flow structures occurring downstream of a sharp-edged bluff body immersed in an open channel flow using three-dimensional numerical simulation. The computational results provide support to previous experimental observations. One of the advantages of the computational model is its ability to capture more information of the flow features at critical locations that could not be acquired by earlier experiments [11].

COMPUTATIONAL SCHEME

A schematic illustration of the flow, along with the co-ordinate system adopted in this study, is shown in Figure 1. The bluff body width is 0.03 m. The unperturbed turbulent boundary layer profile, extracted by conducting a separate simulation for an 8.0 m open channel flow with water depth of 0.1 m, is employed as the inlet boundary condition. As shown in Figure 2, this profile compares well with experimental data as well as the near wall and universal log-law equations. The wall shear stress and friction velocity are estimated to be 0.36 Pa and 0.019 m/s, respectively. The boundary layer thickness is δ = 80 mm, which constitutes 80% of the total depth. The velocity near the free surface is $\mathbf{U}_\infty$ = 0.45 m/s. The Reynolds number is Re ≈ 7500 based on D and $\mathbf{U}_\infty$.

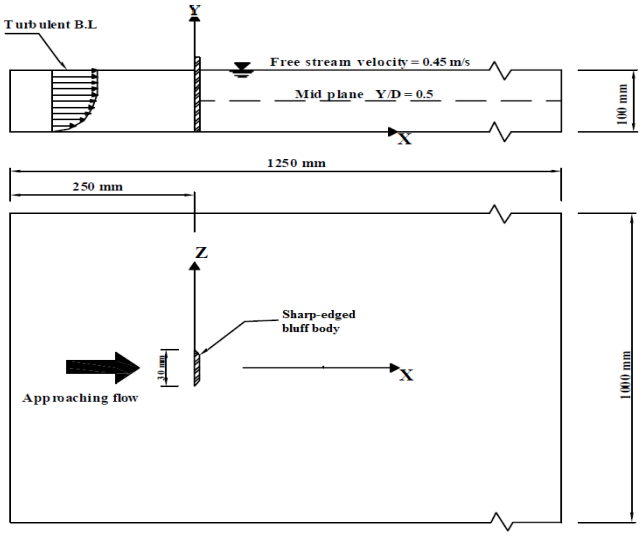

Figure 1 Schematic illustration of the flow

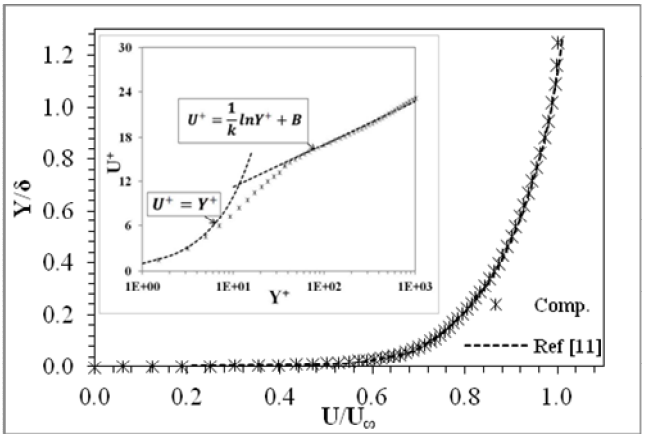

Figure 2 Experimental and computational mean streamwise velocity distribution of the approaching flow

The flow field has been discretized using approximately 3.7M structured elements, taking into account cell clustering near the solid walls and in the wake region. Detached Eddy

Simulation (DES) based on Shear-Stress Transport k-ω SST model was employed as the turbulence model [12]. The DES model is often referred to as a hybrid LES/RANS model. In the DES approach, unsteady RANS models are employed in the near-wall regions. Away from the wall the large scales are resolved, while the subgrid scales are modelled using the same version of the RANS model that is used in the near-wall region. The k-ω SST model in ANSYS Fluent software incorporates modifications for low Reynolds number affects, shears flow spreading and is applicable to wall-bounded flow. Unsteady implicit formulation and second order discretization are used for pressure, momentum, turbulent kinetic energy and specific dissipation equations. The SIMPLE algorithm was employed to solve the pressure-velocity coupling. The values of non-dimensional wall distance Y^+ have been inspected at the near wall locations to ensure it falls within acceptable limits.

VALIDATION OF THE NUMERICAL MODEL

For validation purposes, physical and statistical flow quantities, e.g., mean velocity, turbulence fluctuations, and velocity deficit from the simulation have been compared with experimental data at different vertical locations from the bed, as reported in [11].

Transverse distribution of streamwise velocity deficit is one of the parameters which has been employed to validate the current numerical model. The validation will be presented here, while specific definitions and calculations of the velocity deficit and half-width of the wake can be found in the next section (Results).

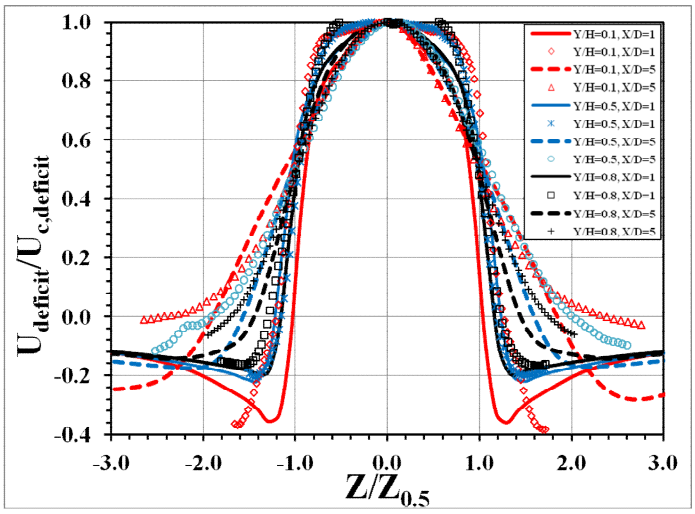

Figure 3 Computational (solid lines) and experimental (symbols) velocity deficit comparison at three horizontal planes; Y/H = 0.1 (red), Y/H = 0.5 (blue) and Y/H =0.8 (black).

As shown in Figure 3, available PIV experimental data have been used to validate the computational results at three different vertical locations from the bed, at Y/H = 0.1, 0.5 and 0.8. In all three planes the computational results are in good agreement with experimental data for $| Z/Z_{0.5} | < 1$ (i.e., in the wake core), with a maximum difference less than 10%. At $| Z/Z_{0.5} | > 1$, the computational and experimental data are still in good agreement in the vicinity of the bluff body for Y/H = 0.5 and 0.8. However, the difference between computational and experimental results increases downstream at the medium-wake region (i.e., 3 < X/D < 6) as one moves towards the edge of the wake.

RESULTS

In this section the averaged and instantaneous statistical quantities for the wake flow field from the CFD simulation are presented and discussed.

The mean velocity distribution provides information on bulk motion of fluid, i.e., convection of fluid particles and relative mixing between different regions in the flow field. Patterns of time-averaged stream traces at different vertical elevations from the bed are given in Figure 4. In this figure, the mean streamwise velocity (U) contour has been superposed on the time-averaged stream traces in the X-Z plane. The effect of bed is obvious on the stream traces topology as shown in Figure 4a, where the recirculation flow is completely suppressed and positive directed velocity dominates the wake flow in this plane. The onset of the reverse flow occurs at vertical location Y/H ≈ 0.1, the formation of a pair of spiralling foci is observed in the near wake region as shown in Figure 4b. The unstable foci are displaced downstream, coupled with expansion of the recirculation region towards the free surface as shown in Figures 4c and 4d.

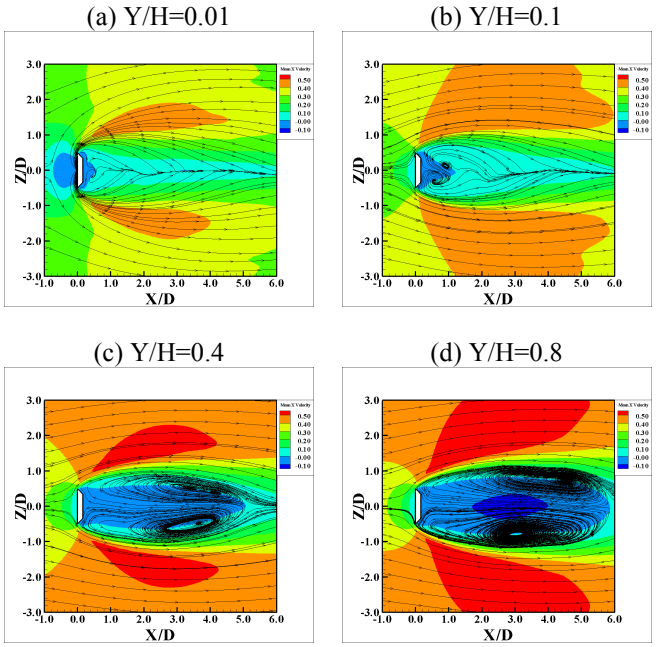

Figure 4 Stream traces of the mean velocity field superposed with mean streamwise velocity (U) for horizontal planes: (a) Y/H = 0.01; (b) Y/H = 0.1; (c) Y/H = 0.4; (d) Y/H = 0.8

More insight into the streamwise velocity development can be realized by examining the streamwise velocity deficit (U_s-$U_{(x,0)}$) distribution along the wake centreline at different locations from the bed. The wake centreline velocity deficit

distribution at different elevations from the bed, normalized with the corresponding upstream velocity (U_s), is given in Figure 5. The kinetic energy is transferred from the outer accelerating flow to the wake where the gradient is negative, and vice-versa where the gradient is positive. A recirculation region (a negative streamwise velocity) in the wake is normally expected where the normalized velocity deficit is greater than unity. Therefore, in the near wake, the energy usually transfers to the wake at locations close to the bed, and from the wake at upper locations. As shown in Figure 5, the downstream distance, where the reverse flow diminishes, increases as the wake moves towards the free surface.

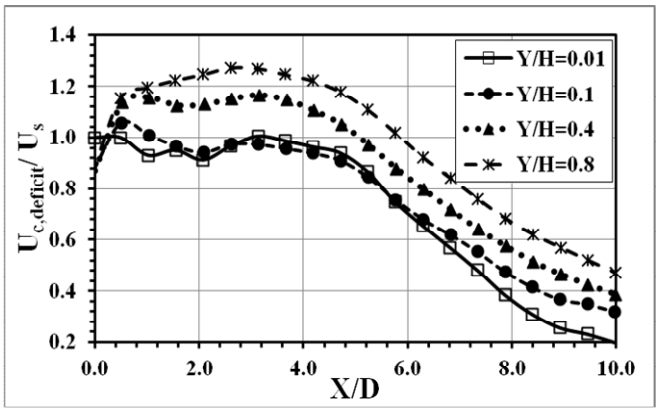

Figure 5 Distribution of the wake centreline velocity deficit at vertical elevations; Y/H =0.01, 0.1, 0.4 and 0.8

Figure 6 shows the transverse distribution of the normalized streamwise velocity deficit ($U_{(x,z)}$ - U_s) / ($U_{(x,0)}$ - U_s) at three different horizontal planes Y/H = 0.1, 0.4 and 0.8, for each plane, the distribution is given at two downstream positions; X/D = 3 and 5. The transverse distance is normalized by the local half width ($Z_{0.5}$), the half-width of wake is defined as the transverse location (Z) where the velocity deficit equals half of the maximum velocity deficit i.e., the velocity deficit in the wake centreline.

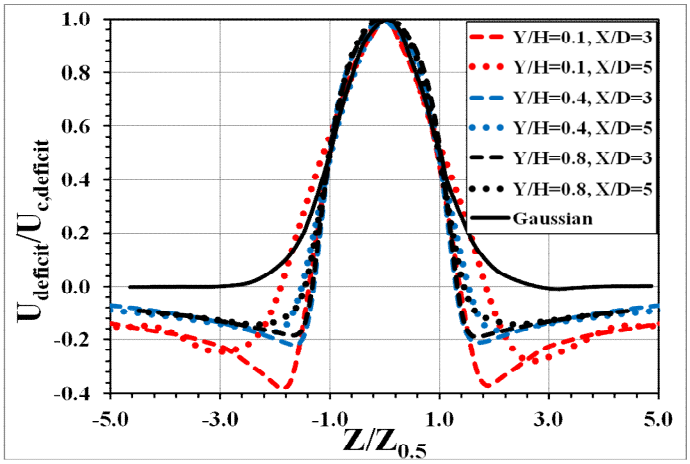

Figure 6 Transverse distribution of the streamwise velocity deficit at three different vertical locations

As shown in Figure 6, the velocity deficit distribution for all horizontal planes spread outwards and approaches the deep flow wake (Gaussian distribution) with increasing downstream distance. At specific downstream distance, the velocity deficit distributions spread wider at locations close to the bed. This observation indicates that the bed friction arrests the transverse growth of the wake, and therefore reduces the half-width close to the bed. However, the damping effect of the bed weakens with increasing distance from the bed.

The contours of the time-averaged vorticity and its streamwise and transverse components are shown in Figure 7, where horizontal and vertical slices were extracted at Y/H = 0.01, 0.4 and 0.8 and X/D = -0.5, 0.5, 2.0 and 3.5 respectively. As shown in Figures 7a and 7d, the vorticity contours of the vortex street extend over the whole depth with a dominant Y-vorticity component. These figures indicate that the size of the vortices tend to be larger as one moves towards the free surface. This demonstrates the effect of the bed, which suppresses the growth of vortices at locations close to the bed.

At the near bed location Y/H=0.01, the counter-rotating streamwise vorticity (red and blue contours) in Figure 7b immediately next to the body and emanating from the edges refer to the separating shear layers. Adjacent to the shear layers are regions of high vorticity generated by the flow negotiating the presence of the body. The vorticity in these regions has a magnitude opposite to that in the adjacent shear layers. The magnitude of these structures (w_x) diminishes as one moves to the upper layers as shown in Figures 7b and 7d.

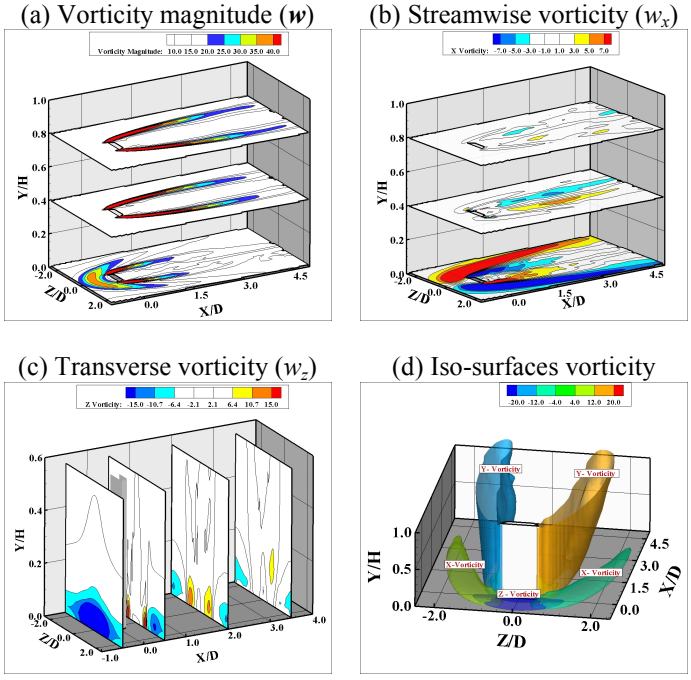

Figure 7 Time-averaged; (a) vorticity magnitude contours; (b) streamwise vorticity component contours; (c) transverse vorticity component contours and (d) iso-surfaces of vorticity components (w_x, w_y and w_z)

The transverse vorticity (w_z) distributions in the Y-Z planes are given in Figure 7c. These patterns clearly indicate the presence of the horseshoe vortex that develops in front of the body at X/D = - 0.5 and extends downstream. The horseshoe vortex envelops the vortices that form part of the vortex street. More insight into the horseshoe vortex can be gained from Figure 7d. In this figure, the iso-surfaces of vorticity components are plotted. Part of the horseshoe vortex (w_z) is captured in front of the body (dark blue surface). The contour of w_z is merged with the streamwise vorticity iso-surface (w_x) which extends downstream.

The counter-rotating streamwise vorticity at the near bed location (Figure 7b) involves upward ejection of fluid through the wake centre (axial flow) as shown in Figure 8. This ejection provides a three-dimensional imprint for the shallow wake. The axial flow does not travel upwards perpendicular to the bed, but at an inclined angle towards the body and transfers the turbulent kinetic energy to the transverse and streamwise components at upper locations from the bed (see also Figure 9a). This observation has been confirmed experimentally in [4]. Comparing the velocity field at three different horizontal locations from the bed reveals that the ejection event is robust in the horizontal plane Y/H = 0.1, and gets weaker with increasing Y/H. At Y/H = 0.9, the velocity vectors exhibit a planar distribution due to the presence of the free surface.

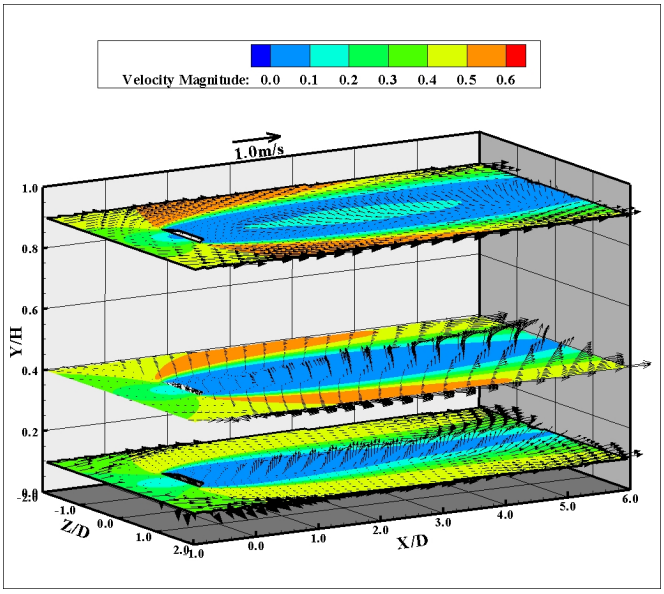

Figure 8 Time-averaged velocity vectors superimposed on contours of time-averaged velocity magnitude at horizontal planes Y/H = 0.1, 0.4 and 0.9

The time-averaged contours of turbulent kinetic energy normalized with the free surface velocity ($\mathbf{U}_\infty$) at three vertical locations Y/H = 0.1, 0.4 and 0.8 are given in Figure 9a. As shown in this figure, the high magnitude kinetic energy contours spread over larger X/D and the wake flow becomes more chaotic as the free surface is approached. Near the bed, the presence of the boundary damps out and alleviates the disorder in the fluid.

The contours of normalized Reynolds stress at different locations from the bed are shown in Figure 9b. The Reynolds stress gives a positive contribution and represents a production term for the turbulent kinetic energy. The Reynolds stress distribution is anti-symmetric with respect to the body, the higher value on each plane stretches along the shoulder of the body. This observation indicates that the momentum exchange by Reynolds stress between the accelerating flow and wake region increases as one approaches the free surface.

(a) Turbulent kinetic energy (b) Reynolds stress

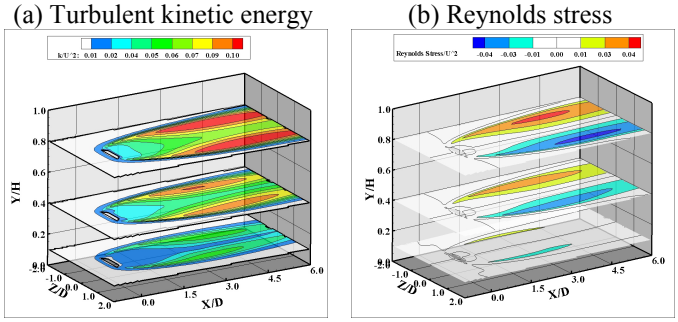

Figure 9 Time-averaged contours of (a) turbulent kinetic energy and (b) Reynolds stress <uw>, extracted at horizontal planes Y/H = 0.1, 0.4 and 0.8

One of the disadvantages in using the time-averaged quantities is that it conceals much of the unsteady characteristics of the flow field. The time dependent quantities divulge more details of the flow field structures. For the current flow, the period of vortex street formation is T ≈ 0.56 sec. The vortex shedding frequency $f \approx 1.8$ *Hz* was calculated using the Fast Fourier Transform (FFT). The Strouhal number based on the width of the body (D) and free stream velocity ($\mathbf{U}_\infty$) is St = 0.2.

The vortical or coherent structures play an important role in understanding many of turbulent features of the flow, e.g., entrainment, mixing, drag. Therefore, there is a need to identify the large-scale vortical regions in turbulent flows. Construction of instantaneous stream trace patterns allows identification of such structures in the flow field. The evolution of instantaneous stream traces topology at different elevations from the bed are given in Figure 10 for two sequential phases of the oscillation cycle at t/T= 0 and 0.6. Each pattern in this figure shows an identifiable focus, which corresponds to the centre of the spiraling stream traces pattern. A further feature in this figure is the existence of well-defined saddle points. The combination of saddle points and a spiral stream traces pattern leads to limiting the cycle of the stream traces and identifies the size of the vortical structures as shown in Figures 10a-10f. The patterns of instantaneous stream traces topology slightly exhibit a slight spatial expansion of the spiraling portion towards the free surface. The size of the large structures in Figure 10 occupy more than 150% of the width of the bluff body, and they appear to meander like a sine wave about the vertical central plane due to interaction between instantaneous vortices and mean flow. Figure 11 shows other selected examples of the large vortical structures extracted at different vertical planes. From this figure, one can identify three type of structures; (1) spiralling

stream trace structures as shown in Figure 11a and 11b, (2) structure with upward flow close to the bed (at X/D = 2.2 and 1.5 in Figures 11a and 11b, respectively) which seems to be due to thrust by streetwise vorticity that resides near the bed and (3) structures that appears as a thick vertical line and span almost the entire water depth as shown in Figure 11c. The direction of the flow at the sides of this element indicates that it is a side-section of a vortical element which resembles a hairpin leg. This shape of the vortical element may be a result of the interaction of a hairpin vortex with quasi-streamwise structures that seem to be common in this kind of flow [13].

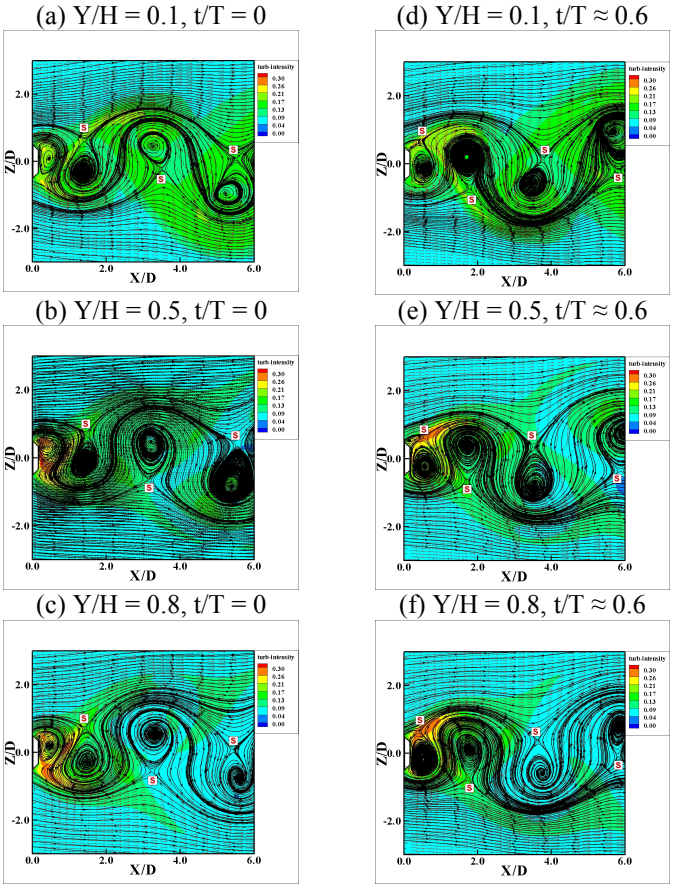

Figure 10 Evolution of the stream traces of instantaneous velocity superposed with turbulence intensity contours at horizontal planes Y/H = 0.1, 0.5 and 0.8

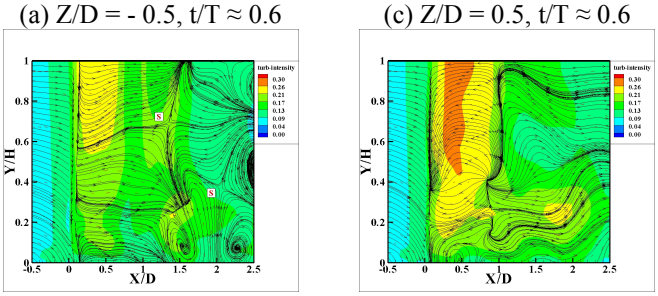

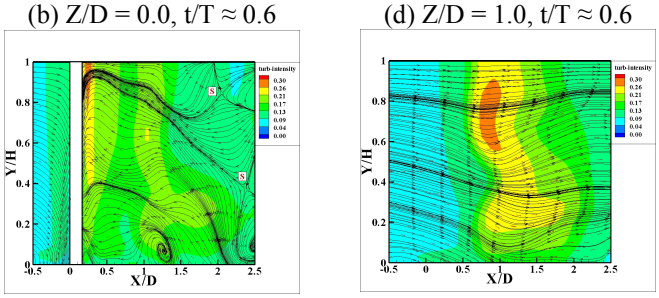

Figure 11 Stream traces of instantaneous velocity superposed with turbulence intensity contours at vertical planes Z/D = -0.5, 0.0, 0.5 and 1.0

CONCLUSIONS

Three-dimension numerical simulation was conducted to study the flow characteristics of the shallow wake flow. The effect of the bed is apparent on the time-averaged topology of stream traces and vorticity at locations close to the wall. A stable narrow wake region associated with positive directed velocity has been found in the centre of the wake in planes close to the bed. The wake region widens with increased recirculation towards the free surface. The formation of a large-scale street vortex involves upward oriented axial flow through the centre of the vortex, this ejection provides a three-dimensional imprint for the shallow wake. A signature of the horseshoe vortex is found at the front of the bluff body at the near bed location.

Comparison of the stream traces topology at different elevations above the bed show that a common saddle point can be identified at approximately the same spatial position in the near and medium wake for all elevations. The vertical and horizontal slices extracted from the instantaneous flow field at different locations reveal the existence of different types of vortical structures.

REFERENCES

[1] Jirka G.H., and Uijttewaal W.S.J., Shallow flows, International Symposium on Shallow Flows, Delft, Netherlands, 2003.

[2] Balachandar, R., Ramachandran, S., and Tachie, M.F., Characteristic of shallow turbulent near wakes at low Reynolds numbers, ASME J.Fluids Engineering, Vol. 122, 2000, pp. 302-308.

[3] Balachandar, R., and Ramachandran, S., Turbulent boundary layers in low Reynolds number shallow open channel flow, ASME J. Fluids Engineering, Vol. 121, 1999, pp. 684-689.

[4] Singha, A., and Balachandar, R., Structure of wake of a sharp-edged bluff body in shallow channel flow, J. Fluids and Structures, Vol. 27, 2010, pp. 233-249.

[5] Chen, D., and Jirka, G.H., Experimental study of plane turbulent wakes in a shallow water layer, Fluid Dynamics Research, Vol. 16, 1995, pp. 11-41.

[6] Akilli, H., and Rockwell, D., Vortex formation from a cylinder at shallow flow, Phys. of Fluids, Vol. 14, 2002, pp. 2957-2967.

[7] Kurosaka, M., Christiansen, J.R., Goodman, W.H., Tirres, L., and Wohlman, R.A., Cross flow transport induced by vortices, AIAA J., Vol. 26, 1988, pp. 1403-1405.

[8] Lin, J.C., Ozgoren, M., and Rockwell, D., Space-time development of the onset of a shallow-water vortex, ASME J. Fluid Mech., Vol. 485, 2003, pp. 33-66.

[9] Rao, S.K., Sumner, D., and Balachandar, R., A visualization study of fluid structure interaction between a circular cylinder and channel bed, J. Visualization, Vol. 7, 2004, pp. 187-199.

[10] Dong, S., Karniadakis, G.E., Ekmerci, E., and Rockwell, D., A combined direct numerical simulation - particle image velocimetry study of turbulent near-wake, ASME J. Fluid Mech., Vol. 569, 2006, pp. 185-207.

[11] Singha, A., Shallow wake in open channel flow - look into the vertical variability, PhD dissertation, 2009, Department of Mechanical, Automotive and Materials Engineering, University of Windsor, Canada.

[12] ANSYS Fluent Inc., User's Guide, 2011.

[13] Singha, A., Shinneeb, A., and Balachandar, R., PIV-POD investigation of the wake of a sharp-edged flat bluff body immersed in a shallow channel flow, ASME J. Fluid Eng., Vol. 131, 2009, pp. 233-249.